Surface Observations in the Hurricane Environment

JOSEPH J. CIONE, PETER G. BLACK, AND SAMUEL H. HOUSTON

National Oceanic and Atmospheric Administration, Atlantic Oceanographic and Meteorological Laboratory,
Hurricane Research Division, Miami, Florida

ABSTRACT

Composite analyses of marine surface observations from 37 hurricanes between 1975 and 1998 show that the difference between the sea surface temperature and the surface air temperature significantly increases just outside the hurricane inner core. This increase in the sea–air contrast is primarily due to a reduction in surface air temperature and is more likely to occur when sea temperatures are at least 27°C. Results show that 90% of the observed cooling occurs 3.25°–1.25° latitude from the hurricane center, well outside the region of strongest surface winds. Since surface pressure only decreases 3 mb over this interval, the ~2°C drop in air temperature is not a result of adiabatic expansion.

For the subset of observations that contained moisture measurements, surface specific humidity decreased 1.2 g kg^{-1} 4.5°–1.75° latitude from the storm center. This finding suggests that the observed reduction in surface air temperature is not simply a result of near-surface evaporation from sea spray or precipitation. An alternate explanation may be that outside the hurricane inner core, unsaturated convective downdrafts act to dry and evaporatively cool the near-surface environment.

Between 3.25° and 1.25° radius, composite analyses show that low-level inflow is not isothermal, surface moisture is not constant, and the near-surface environment is not in thermodynamic equilibrium with the sea. Calculations based on these observations show that θ_e decreases between 4.0° and 1.25° radius and then quickly rises near the inner core as surface pressures fall and specific humidity increases. Surface fluxes of heat and moisture are also observed to significantly increase near the inner core. The largest increase in surface sensible heat flux occurs radially inward of 1.5°, where surface winds are strong and sea–air temperature contrasts are greatest. As a result, the average Bowen ratio is 0.20~0.5° radius from the composite storm center. This increase in sensible heat flux (in conjunction with near-saturated conditions at low to midlevels) may help explain why average surface air temperatures inside 1.25° radius remain relatively constant, despite the potential for additional cooling from evaporation and adiabatic expansion within the high wind inner core.

1. Introduction

Low-level observations near and within the hurricane inner core have been rare. The lack of data in this region has forced researchers to make assumptions regarding the thermodynamic structure of the tropical cyclone (TC) boundary layer, including the critically important air–sea interface where ocean–atmosphere exchanges of momentum, heat, and moisture occur. Based on a few observations, it is the "conventional wisdom" that differences between sea surface temperature (SST) and surface air temperature (TA) within the hurricane environment are small (i.e., SST − TA ~ 0°–1°C) and do not vary much as a function of distance from the storm center (Byers 1944; Palmen 1948; Riehl 1950, 1954; Miller 1958; Gray and Shea 1973; Hawkins and Im-

bembo 1976; Holland 1987; Willoughby 1995). It has also been speculated that any adiabatic or evaporative cooling experienced by surface air parcels as they flow inward toward lower pressure will be effectively balanced by heat transfer from the sea or by downward vertical mixing of relatively warm air above the surface (Byers 1944; Malkus and Riehl 1960; Frank 1977, 1984; Barnes and Powell 1995). Assumptions about SST − TA are particularly essential to thermodynamic models attempting to simulate the structure and physical processes responsible for the evolution and maintenance of hurricanes (Emanuel 1986; Holland 1997).

Recent studies by Korolev et al. (1990), Pudov (1992), and Pudov and Holland (1994) suggest, however, that there may be some functional dependence of the sea–air temperature contrast on the surface wind speed. Korolev et al. (1990) and Pudov (1992) observed that the average sea–air contrast (SAC) for two tropical storms increased from 1°C to 5°–6°C as surface wind speed increased from 12 to 25 m s^{-1}. They suggested that the reduction in TA occurred primarily due to the evaporation of sea spray and that this cooling was dra-

matically enhanced as the sea state rose in response to stronger surface winds. While these preliminary findings are significant, a more thorough investigation using observations from many storms (particularly hurricanes) is essential if we are to understand air–sea interaction processes that regularly occur in tropical systems. A major objective of this research is to construct multistorm composite analyses of near-surface atmospheric and oceanic conditions in order to improve the physical representation and basic understanding of the low-level thermodynamic environment observed in hurricanes.

2. Observational database

This research utilizes over 7800 individual near-surface meteorological and oceanographic observations from the National Data Buoy Center's (NDBC) moored and drifting buoys and coastal marine automated network (C-MAN) platforms. The tropical cyclone–buoy database (termed TCBD) developed for this study includes 153 time series from 37 hurricanes over a 23-year period between 1975 and 1998 (Table 1). In order for a buoy–C-MAN time series to be incorporated in the TCBD, at least one observation must come within 250 km of the hurricane center. In addition, only surface data within 6° radius of the storm center have been included.

Hourly observations of standard surface meteorological data [TA, sea level pressure (SLP), wind speed and direction] were obtained from marine observing platforms for the 37 hurricanes illustrated in Table 1. Many of the time series in the TCBD also recorded measurements of SST. For 10 of the 37 hurricanes studied, surface dewpoint temperature (TD) was available. Most of the TCBD observations were acquired from NDBC's quality controlled online archive buoy database (Gilhousen 1988, 1998). Detailed information on items such as platform locations and configurations, sensor descriptions and levels of accuracy, data acquisition, averaging, quality control, and archival techniques is available at the NDBC Internet site (http://www.noaa.ndbc.gov).

Over the past two decades, efforts by the Hurricane Research Division (HRD) have improved the quality of the current buoy–C-MAN database maintained at NDBC. This long-term quality control effort has been important in identifying and removing questionable surface data, particularly from the 1970s and early 1980s. In addition to these important contributions, considerable work has gone into improving the TCBD used in this research. This includes the elimination of several C-MAN time series that did not represent a marine exposure environment as well as efforts designed to identify possible cases of "wet-bulb" contamination within the TCBD. Wet-bulbing occurs when a thermistor becomes wet, and evaporative cooling on the sensor results in an erroneously cool TA measurement. Since only 10 of the 37 storms had TD observations, low-level moisture measurements could not always be used to detect

TABLE 1. Hurricanes in the tropical cyclone–buoy database.

Hurricanes	Year	Hurricane center fix: best track = BT, enhanced track = ET	Total no. of time series	No. of surface dewpoint (TD) time series
Georges	1998	BT	11	2
Earl	1998	ET	7	1
Bonnie	1998	ET	10	0
Danny	1997	BT	3	2
Fran	1996	ET	8	1
Bertha	1996	ET	4	1
Edouard	1996	ET	6	0
Hortense	1996	ET	1	0
Marilyn	1995	BT	6	0
Luis	1995	BT	3	0
Felix	1995	ET	5	1
Allison	1995	BT	2	0
Opal	1995	ET	6	1
Erin	1995	BT	4	0
Gordon	1994	ET	8	1
Emily	1993	ET	7	0
Andrew	1992	ET	7	0
Iniki	1992	BT	2	0
Bob	1991	ET	13	1
Hugo	1989	ET	5	0
Jerry	1989	BT	1	0
Gilbert	1988	BT	1	0
Elena	1985	ET	1	0
Gloria	1985	ET	10	0
Kate	1985	BT	2	0
Danny	1985	BT	1	0
Juan	1985	BT	1	0
Josephine	1984	BT	3	0
Alicia	1983	BT	1	0
Allen	1980	BT	2	0
David	1979	BT	2	0
Frederic	1979	ET	2	0
Bob	1979	BT	1	0
Ella	1978	BT	1	0
Anita	1977	ET	2	0
Belle	1976	ET	2	0
Eloise	1975	ET	2	1

the occurrence of near-surface wet-bulbing. Nevertheless, by using existing paired observations of TA and TD, preliminary analyses designed to investigate the occurrence of wet-bulbing could be attempted. For this analysis, TA and TD at $t = t_0$ were compared with TA and TD observations at $t = t_0 + 1$ h. As such, 1-h "ΔTA" and "ΔTD" pairings were determined. After eliminating all observations having surface winds <13 m s^{-1}, 418 ΔTD–ΔTA pairings remained. Of these, 45 exhibited TA reductions $<-0.5°$C h^{-1}. If wet-bulbing were occurring in these cases, an increasing trend in TD (i.e., positive ΔTD values) would be expected. However, for the 45 strongest cooling events the average ΔTD was found to be $-0.26°$C h^{-1}. Using a Student's t-test, the difference between the population ΔTD mean of $-0.04°$C h^{-1} and the 45-member sample mean of $-0.26°$C h^{-1} was found to be statistically significant beyond the 5% level. A brief summary of this analysis is given in Table 2. These findings suggest that low-

TABLE 2. Statistical summary of paired Δ TA–Δ TD observations.

Statistics given in °C	ALL Δ TA	ALL Δ TD	Δ TA < −0.5°C	Δ TD (Δ TA < −0.5°C)	Δ TA < −0.5°C top 25%	Δ TD (Δ TA < −0.5°C top 25%)
Min	−2.1	−2.7	−2.1	−2.0	−2.1	−2.0
Max	1.2	2.3	−0.6	1.2	−1.2	0.9
Sum	−27.3	−18.0	−44.0	−11.5	−20.3	−7.5
Range	3.3	5.0	1.5	3.2	0.9	2.9
Mean	−0.065	−0.043	−0.978	−0.256	−1.562	−0.577
Std dev	0.450	0.601	0.413	0.705	0.273	0.881
Count	418	418	45	45	13	13

level drying (and not wet-bulbing) is associated with the strongest surface cooling events observed in the TCBD. The issue of low-level drying and cooling will be discussed further in section 3b.

All surface winds used in the TCBD have been referenced to a 1-min averaging period using standard overwater ratios. Since NDBC observations use 8.5-min averaging periods for hourly buoy observations, 10-min averaging periods for drifting platform data, and 2-min averaging periods for observations obtained at C-MAN platforms, surface winds were normalized to a common maximum 1-min sustained averaging time (Powell et al. 1996). The 1-min period was chosen since it is the same averaging period used in advisories issued by the National Hurricane Center. In addition, all winds in the TCBD were adjusted to a common reference height of 10 m (Liu et al. 1979). For platforms that recorded TA at heights other than 10 m, a dry-adiabatic lapse rate adjustment to 10 m was made (i.e., ±0.0098°C m⁻¹). No corrections were made for differences between SST and TA.

In addition to using hurricane positions obtained every 6 h from the "best track" dataset (Neumann et al. 1993), center fixes were also obtained from National Oceanic and Atmospheric Administration WP-3 and U.S. Air Force Reserves WC-130 aircraft reconnaissance flight missions. These high temporal "enhanced" TC center positions were available for 19 of the 37 hurricanes listed in Table 1.

3. Near-surface thermodynamic observations in hurricanes

a. Radial variations in sea–air contrast and surface wind speed

Figures 1a, 1b, and 1c are scatterplots of SAC for the SST ≥27°C subgroup (herein referred to as the ≥27 group), SAC for the SST <27°C group, and the 10-m wind speed for the ≥27°C group, respectively. Observations illustrated in Figs. 1a–c were subject to minimum surface wind speed thresholds of 13 m s⁻¹ beyond 0.75° radius from the hurricane center and 17.5 m s⁻¹ inside 0.75° radius from the center. The 13 m s⁻¹ threshold was chosen since it incorporated most observations but eliminated a few suspect low wind cases. The latter

filter of 17.5 m s⁻¹ inside 0.75° radius was designed to eliminate surface observations within the hurricane eye.

After stratifying surface observations by SST ≥ or < 27°C, it was apparent that SACs for the ≥27 group noticeably increased with decreasing radial distance. This trend was not found for the <27 group shown in Fig. 1b. Figures 1a and 1b also illustrate that the degree of variability in SAC was much greater for the <27 group. In fact, the difference in standard deviation between these two groups was shown to be statistically significant beyond the 1% level (Table 3). Table 3 gives a summary of the SAC radially binned observations for both the ≥27 and the <27 groups. In addition, Table 3 illustrates statistics for SLP, SST, and TA as well as the mean and radially dependent values of surface wind speed for the ≥27 group.

Figures 1a and 1b depict contrasting low-level thermodynamic conditions near the inner core. In Fig. 1a, 294 of the 298 observations (i.e., 99%) exhibit SACs >0°C inside 2° radius. In contrast, less than 50% of the 234 observations inside 2° radius in Fig. 1b have SAC values >0°C. One possible reason for the increased variability and lower SACs in Fig. 1b may be found in Table 3. Here, we see that the average latitude for observations in Fig. 1b is 34.8°N versus 28.3°N for observations shown in Fig. 1a. In Fig. 1b, the observations are more likely to have come from northward "recurving" hurricanes located off the U.S. east coast. As such, these storms would tend to encounter significantly cooler SSTs poleward of the Gulf Stream "north wall" (typically located between 35° and 37°N, west of 65°W).

Counter to the Korolev et al. (1990) and Pudov (1992) case study results shown in Fig. 2a, the 1967 TCBD observations illustrated in Fig. 2b only suggest a weak positive correlation between the SAC and the surface wind speed. Less than 8% of the variance is explained for the polynomial fit illustrated in Fig. 2b. When observations having SSTs ≥27°C and surface wind speeds >13 m s⁻¹ outside 0.75° radius or >17.5 m s⁻¹ inside 0.75° radius were used, only 17% of the observed variance was explained (not shown). In comparison, 40% of the variance is explained for the polynomial fit shown in Fig. 1a between the SAC and the radial distance from the hurricane center.

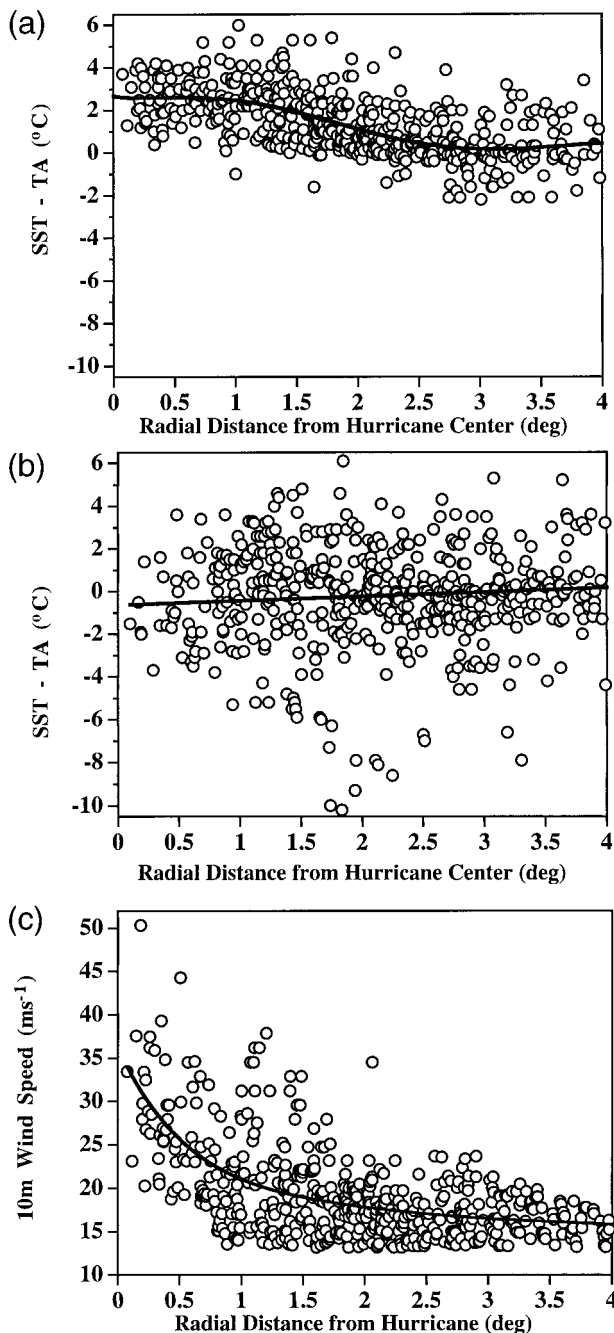Radially binned TCBD values illustrated in Table 3

FIG. 1. (a) Scatterplot of the SST minus the TA, or SAC, as a function of radial distance from the hurricane center for all buoy or coastal marine automated network observations with SSTs at least 27°C and surface wind speeds >13 m s^{-1} outside 0.75° radius or >17.5 m s^{-1} inside 0.75° radius. SSTs and TAs are given in °C. A polynomial best-fit curve is also illustrated and is given by the following equation $y = 0.033x^3 - 0.114x^2 - 0.911x + 3.025$. For this fit, over 40% of the variance is explained ($R^2 = 0.401$). (b) Same as in (a) except all observations illustrated exhibit SSTs <27°C. Unlike (a), little variance is explained. A linear best-fit is illustrated. (c) Same as in (a) except observations depict the 10-m 1-min surface wind speed. Surface wind speeds are given in m s^{-1}. As in (a), a polynomial best-fit curve has been applied. The polynomial is given by $y = -0.370x^3 + 3.842x^2 - 13.262x + 31.585$ and explains 46.2% of the observed variance.

show that much of the observed increase in SAC is a result of TA cooling occurring ~3.25°–1.25° radius from the storm center, well outside the region of strongest surface winds and maximum pressure gradients. In order to determine if the average increase in SAC from 0.15°C (~3.25° radius) to 2.42°C (~1.25° radius) illustrated in Table 3 was statistically significant, a Student's t-test that assumed unequal variance was conducted. Italic values in Table 3 signify a statistically significant difference (at the 1% level) with the adjacent mean value radially outward. Results from this analysis show that true differences between mean SAC values of 0.99°C (~2.25° radius) and 1.75°C (~1.75° radius), and 1.75°C (~1.75° radius) and 2.42°C (~1.25° radius) existed in each case beyond the 1% significance level. Similar statistical analyses showed that the increase in surface wind speed from 16.6 to 20.4 m s^{-1} between 3.25° and 1.25° radius was not found to be statistically significant at the 1% level in any case. It should be noted that the rise in SAC between 3.25° and 1.25° radius represents 96% of the total 2.4°C SAC increase observed inside 3.5° radius. In contrast, the increase in surface wind speed from 16.6 to 20.4 m s^{-1} over this same interval only represents 32% of the total 11.9 m s^{-1} wind speed increase observed inside 3.5° radius.

Radially binned averages of the parameters shown in Table 3 for the ≥27 group are also illustrated in Figs. 3a–c. Figure 3a depicts the SAC, SST, and TA, Fig. 3b shows the 10-m surface wind speed and 10-m radial wind, and Fig. 3c illustrates SLP and TA$_{adiabatic}$, where TA$_{adiabatic}$ represents the impact of adiabatic expansion on the surface air parcel as it encounters lower pressure. Figures 3a and 3c show that only 0.3°C of the 1.9°C TA decrease between 3.25° and 1.25° radius is attributable to adiabatic expansion resulting from reduced SLP. Figures 3a–c also show, that on average, only 0.2°C additional TA cooling is observed within the high wind inner core despite rapidly falling SLPs and associated TA$_{adiabatic}$ reductions on the order of 1.8°C inside 1.25° radius.

b. Radial variations in low-level moisture

A possible explanation for the TA decrease observed in Fig. 3a may be found in Fig. 4, which illustrates radially binned calculations of surface relative humidity (RH) and surface specific humidity (q). These calculations are based upon direct measurements of TD from 10 of the 37 TCBD hurricanes listed in Table 1. In addition to the radially averaged values shown in Fig. 4, a statistical summary of these moisture parameters is given in Table 4. As with previous illustrations, only observations with SSTs ≥27°C and surface wind speeds >13 m s^{-1} outside 0.75° radius or >17.5 m s^{-1} inside 0.75° radius were included. It is evident from Fig. 4 that RH and q vary as a function of radius [despite earlier studies suggesting otherwise (Miller 1958; Gray and Shea 1973)]. Figure 4 shows that a temporary reduction

TABLE 3. Statistical summary of radially binned surface observations. Italic values indicate statistical significance at the 1% level with the next radial bin going outward.

Parameters	All obs	0°–0.5° lat	0.5°–1.0° lat*	1.0°–1.5° lat	1.5°–2.0° lat	2.0°–2.5° lat	2.5°–3.0° lat	3.0°–3.5° lat	3.5°–4.5° lat	4.5°–6.0° lat
			Obs w/SST $\geq$ 27°C							
			Avg. lat. 28.3°N, Avg. long. 82.2°W							
Sea–air contrast (°C)										
Min	−2.2	0.4	0.4	−1.0	−1.6	−1.4	−1.1	−2.2	−2.1	−1.5
Max	6.0	4.2	5.2	6.0	5.4	4.4	4.9	3.9	3.8	3.1
Mean	1.23	2.54	2.44	*2.42*	*1.75*	0.99	0.55	0.15	0.41	0.34
Std dev	1.45	1.08	1.08	1.32	1.34	1.07	1.07	1.05	1.29	0.99
Count	738	37	69	85	107	128	91	80	84	57
Sfc wind (m s⁻¹)										
Min	13.2	18.7	13.5	13.5	13.2	13.2	13.2	13.3	13.2	13.2
Max	50.4	50.4	44.3	37.9	32.9	34.5	23.7	23.7	26.6	18.4
Mean	18.58	*28.48*	22.28	20.41	18.65	17.76	16.57	16.60	16.39	15.07
Std dev	5.02	6.74	5.85	5.75	4.47	2.82	2.37	2.68	2.51	1.13
Count	751	37	73	89	110	129	91	81	84	57
Sfc radial wind (m s⁻¹)										
Min	−46.2	−46.2	−27.7	−27.9	−24.7	−23.3	−17.0	−16.3	−19.8	−14.9
Max	25.2	25.2	21.5	7.9	13.4	12.0	16.6	19.7	22.9	8.3
Mean	−6.40	−4.8	−8.1	−7.9	−6.3	−7.0	−4.9	−6.7	−5.8	−4.6
Std dev	7.82	16.05	8.75	7.98	7.45	5.88	7.36	6.80	7.0	5.40
Count	745	36	72	88	110	127	91	80	84	57
Sea level press (mb)										
Min	946.6	946.6	966.4	980.0	987.8	987.2	992.8	993.2	983.2	995.6
Max	1015.4	1003.6	1009.8	1012.0	1013.0	1013.0	1013.8	1013.4	1014.3	1015.4
Mean	1002.5	*980.5*	*997.5*	1001.6	1002.5	1004.4	1006.0	1005.3	1004.6	1006.6
Std dev	8.96	14.91	9.99	8.27	6.24	4.86	4.46	5.53	6.55	5.01
Count	738	36	69	85	107	128	91	81	84	57
SST (°C)										
Min	27.0	27.1	27.1	27.0	27.0	27.0	27.0	27.0	27.0	27.0
Max	29.9	29.5	29.8	29.9	29.7	27.9	29.7	29.3	29.7	29.6
Mean	28.15	28.25	28.49	28.31	28.17	27.95	27.97	27.88	28.17	28.44
Std dev	0.74	0.72	0.79	0.75	0.78	0.69	0.66	0.54	0.70	0.80
Count	751	37	73	89	110	129	91	81	84	57
Air temp (°C)										
Min	22.7	23.0	23.1	23.4	22.7	23.6	23.4	25.1	24.5	24.0
Max	29.8	28.5	28.8	28.8	29.6	29.6	29.5	29.8	29.7	29.6
Mean	26.92	25.71	25.93	*25.89*	*26.43*	26.96	27.33	27.74	27.76	28.10
Std dev	1.42	1.20	1.13	1.30	1.42	1.23	1.17	1.01	1.15	1.02
Count	738	37	69	85	107	128	91	80	84	57
			Obs w/SST <27°C							
			Avg. lat. 34.8°N, Avg. long. 75.2°W							
Sea–air contrast (°C)										
Min	−10.2		−3.8	−5.3	−10.0	−10.2	−7.0	−5.0	−7.9	−3.7
Max	6.1		3.6	4.6	4.8	6.1	4.3	5.3	5.2	6.1
Mean	−0.24		−0.41	0.33	−0.65	−0.58	−0.27	−0.35	0.19	0.44
Std dev	2.32		1.90	2.24	2.95	2.79	1.85	2.02	2.07	2.15
Count	645		67	88	79	98	79	87	96	51

* For observations where SST is <27°C, the 0.5°–1.0° lat column represents all observations 0–111 km from the hurricane center.

in near-surface moisture exists between 4.5° and 1.75° radius. The difference between the mean q values of 20.2 g kg⁻¹ (between 5° and 3.5° radius) and 19.0 g kg⁻¹ (between 2.25° and 1.5° radius) illustrated in both Table 4 and Fig. 4 is statistically significant beyond the 5% level. Figure 4 also depicts a dramatic increase in q inside ~1.25° radius from the storm center. Using a Student's t-test for unequal variance, the average increase in q from 19.0 to 20.5 g kg⁻¹ (inside 0.75° radius) is statistically significant well beyond the 1% level.

In section 2 it was shown that hourly reductions in TA <−0.5°C were associated with decreases in TD. From Table 2, we also see that the average drop in TD for the 13 strongest surface cooling events (i.e., top 25% of the ΔTA <−0.5°C sample) was −0.58°C. This compares with a −0.04°C mean drop in TD for the entire ΔTD population. Even after accounting for the low sample size, the likelihood of a true difference between these two means is greater than 95%. For these pairings, over 35% of the variance is explained ($R^2 = 0.351$).
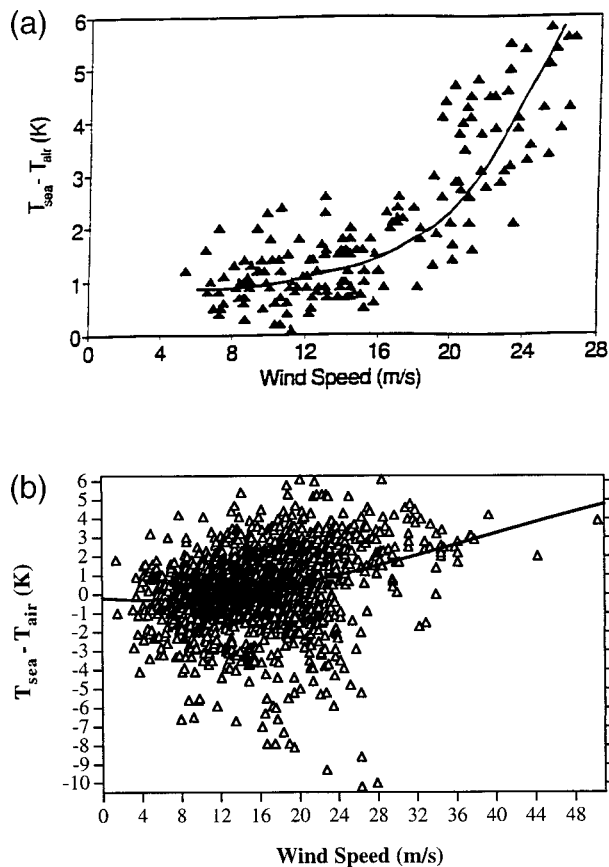
(a)

(b)

FIG. 2. (a) The difference between sea temperature (T_{sea}) and surface air temperature (T_{air}) (in K) vs surface wind speed (in m s^{-1}) taken from the research ship *Priliv* in 1988. The illustration is taken from Fairall et al. (1994), who modified the plot from Pudov (1992). (b) Same as in (a) except that $T_{sea} - T_{air}$ values and surface wind speeds are from the tropical cyclone boundary layer database. The 1967 observations illustrated are ≤5° latitude from the composite TC center. The third-order polynomial curve fit illustrated is given by $y = -4.5 \times 10^{-5}\, x^3 + 5 \times 10^{-3}\, x^2 - 0.041x - 0.21$ and explains 7.7% of the observed variance between changes in sea–air contrast and the surface wind speed.

(a)

(b)

(c)

FIG. 3. (a) Radially-averaged values of SST − TA (solid line–open circles), SSTs (dashed line–open boxes), and TA (heavy dashed line–open triangles) as a function of radius. (b) The radially averaged, 10-m 1-min (total) surface wind speed (solid line–open circles) and (the negative) radial component of the 10-m surface wind (dashed line–open boxes) inside 4.0° radius. (c) The radially averaged, composite SLP (solid line–open circles) and TA due to adiabatic expansion (dashed line–open boxes) as a function of radius. SSTs, TAs, SLPs, and wind speeds are given in °C, °C, mb, and m s^{-1}, respectively.

These statistical results suggest that some of the strongest cooling events observed in the TCBD may be associated with concurrent episodes of low-level drying. This trend is also illustrated in Fig. 5a, which depicts a portion of the paired TA–TD time series obtained from the Sombrero Key (SMKF1) C-MAN platform during Hurricane Georges (1998). The rapid drops in TA and TD observed between 2200–2300 UTC on 24 September 1998 are associated with a strong line of convection that moved through the SMKF1 station during that period (Fig. 5b). It should be noted that this particular ΔTA–ΔTD pairing was not included in the statistical analysis since the minimum wind speed threshold was not met at 2200 UTC. Nevertheless, these illustrations in conjunction with paired TA–TD statistical analyses suggest that low-level drying may accompany significant cooling events near regions of active convection.
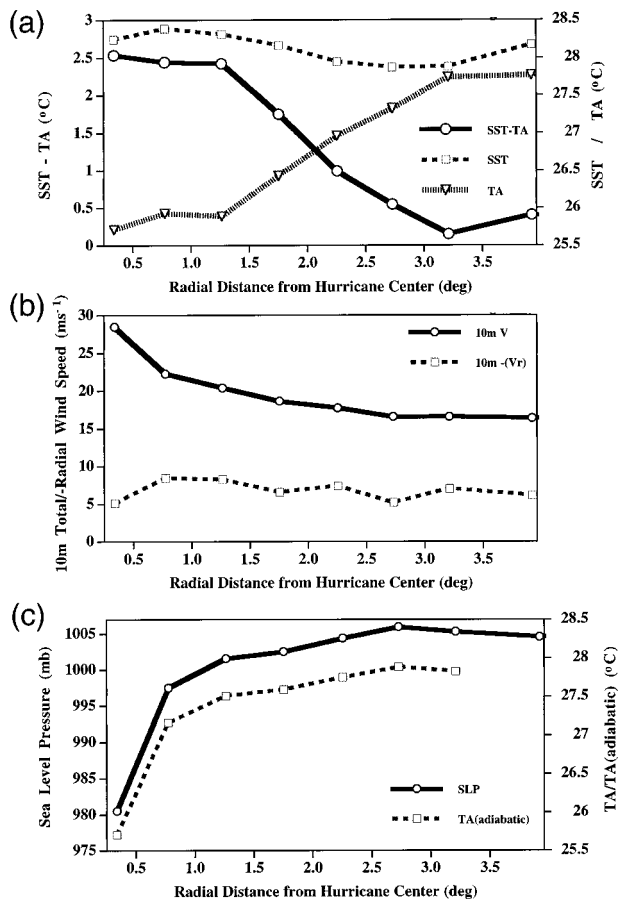
These findings are significant since convective downdrafts are capable of bringing cooler air to the surface via evaporation, provided the air aloft is sufficiently dry (Barnes et al. 1983; Powell 1990). This "necessary condition" is more likely to be met outside the hurricane inner core where drier conditions in the low to midtroposphere are more common (Frank 1977). The composite analysis of near-surface moisture illustrated in Fig. 4 also demonstrates that drier conditions are observed away from the inner core ~1.0°–3.0° radius from the hurricane center. These results may help explain why the majority of TA cooling is observed well away from the storm center (Fig. 3a). Within this outer region, dry air at low to midlevels could potentially modify TA and q structure in and around areas of active convection (Barnes et al. 1983; Powell 1990). However, within the highly convective inner core, it is likely that conditions
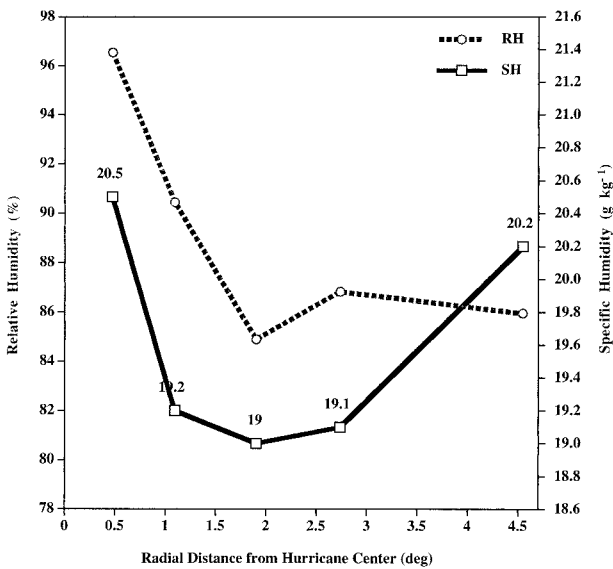
FIG. 4. The radially-averaged, relative humidity (RH) (dashed line/open circles) and surface specific humidity (q) (solid line/open boxes). RH and q are given in % and g kg⁻¹, respectively. Value labels for q are also illustrated.

Earlier studies investigating tropical squall-line convective systems have documented the fact that convective-scale downdrafts often interact with the tropical boundary layer (Betts 1976; Zipser 1977; Johnson and Nichols 1983; Fitzgarrald and Garstang 1981a,b). These studies also showed that relatively cool and dry squall-line wakes existed for several hours and were often readily discernable over hundreds of square kilometers. In Hurricanes Earl (1986) and Josephine (1984), Powell (1990) confirmed that convective downdrafts associated with hurricane rainbands transported dry air to the surface. In addition to these observational studies, numerical simulations conducted by Brown (1979) and Leary (1980) showed that downdrafts associated with tropical squall line convection significantly modified the thermodynamic structure of the tropical boundary layer by injecting relatively dry air into it. In each of these studies, the post-rainband–squall line tropical boundary layer was drier and noticeably cooler when compared with the initial, undisturbed, low-level environment (Barnes et al. 1983; Powell 1990).

aloft are well mixed and closer to saturation (Frank 1977; Jorgensen 1984). Under these conditions, the potential for downdraft-induced TA cooling would be significantly reduced (Barnes and Stossmeister 1986). TCBD composite analyses showing increasing q and constant TA inside 1.25° radius tend to support these findings (Figs. 4 and 3a).

c. Radial variations in θ_e

Over the last three decades, few surface moisture observations have been made in hurricanes over the ocean. However, if the overall "U-shaped structure" of q illustrated in Fig. 4 proves to be representative as additional measurements become available, the implications are significant. Figure 6 represents a radial depiction of θ_e using mean SLP and TA values from Table 3 with q

TABLE 4. Statistical summary of surface moisture parameters.

Parameters	0°–0.75° lat	0.75°–1.5° lat	1.5°–2.25° lat	2.25°–3.5° lat	3.5°–5° lat
Obs w/SST > 27°C					
Specific humidity (g kg⁻¹)					
Min	18.4	17.2	17.4	16.4	15.9
Max	22.1	21.6	21.3	21.2	23.3
Mean	20.5	19.2	19.0	19.1	20.2
Std dev	1.1	1.3	1.4	1.3	1.9
Count	14	22	14	16	20
RH (%)					
Min	79.7	78.7	73.5	79.2	78.1
Max	100.0	100.0	100.0	98.2	95.2
Mean	96.5	90.5	84.9	86.8	86.0
Std dev	5.41	6.14	8.62	7.04	4.34
Count	14	22	14	16	20
Sensible heat flux (W m⁻²)					
Min	17	−48	−59	−100	−85
Max	813	363	285	276	115
Mean	220	115	62	18	13
Std dev	139	85	63	42	38
Count	61	129	168	255	110
Latent heat flux (W m⁻²)					
Min	550	313	208	221	192
Max	1992	1542	984	671	588
Mean	1108	721	564	434	427
Std dev	482	346	215	137	122
Count	14	22	14	16	20

values shown in Fig. 4 (interpolated to the radii used in Figs. 3a–c).

It was noted by Simpson (1978) that traditional estimates of θ_e can lead to errors of several degrees Kelvin in the Tropics. For the analysis illustrated in Fig. 6, an improved, empirically derived approximation for θ_e (Bolton 1980) was used. This formulation is given by

$$\theta_e = \theta \exp[(3.376/T_{\mathrm{LCL}} - 0.002\,54)$$
$$\times 1000q(1 + 0.81q)], \qquad (1)$$

where q is the surface specific humidity, T_{LCL} is the temperature (in K) at the lifted condensation level (LCL), and θ is the potential temperature of the surface air parcel, also given in degrees Kelvin. The temperature at the LCL can be computed by an empirical relationship accurate to within 0.1 K (Bolton 1980; Holland 1997):

$$T_{\mathrm{LCL}} = [2840/(3.5 \ln T - \ln e - 4.805)] + 55, \quad (2)$$

where T is the surface air temperature (in K) and e is the water vapor pressure measured in millibars.

In addition to the θ_e profile determined using TCBD observations, Fig. 6 also depicts an "assumed" θ_e profile that uses a prescribed near-surface inflow temperature of SST $- 1°$C as well as a constant RH of 85%. The thermodynamic basis of the assumed profile is a balance between cooling from adiabatic expansion as the parcel flows inward and heating from the sea and/or from entrainment of relatively warm air above the cloud base (Malkus and Riehl 1960; Frank 1977, 1984; Willoughby 1995; Barnes and Powell 1995). The value of 85% is used since it is an often-cited reference value for RH in the hurricane near-surface inflow layer (Miller 1958; Willoughby 1995). Previous use of a constant 85% RH may have arisen from the "linear extrapolation" of results from an observational study conducted by Jordan (1958), showing surface RHs to be ~80%–85% in the undisturbed Tropics with observations obtained from research and reconnaissance flights suggesting average surface RHs in the hurricane eye to be on the order of 80%–90% (Jordan 1952).

Figure 6 shows a decreasing trend in "observed" θ_e between ~4.0° and 1.25° radius, stemming from inward reductions in both TA and q. In contrast, Fig. 6 depicts a marginal increase in "assumed" θ_e over this same interval as prescribed values of TA and q remain relatively constant and mean SLP decreases 3 mb from 1004.6 to 1001.6 mb. The net θ_e increase between 4.0°– 1.25° radius for the assumed profile is 1.2 K while the observed θ_e decrease is slightly more than 4.1 K between 4.0°–1.25° radius. Similar to earlier studies depicting low-level radial profiles of θ_e near the inner core (Jorgensen 1984; Barnes and Stossmeister 1986; Barnes and Powell 1995), both profiles in Fig. 6 show an increasing trend in θ_e inside 1.25° radius. Figure 6 illustrates an 8-K increase in observed θ_e and a 3.4-K increase for the assumed profile. While both profiles exhibit θ_e increases resulting from reductions in SLP near

the inner core (997.5 to 980.5 mb), only the observed θ_e profile includes the effects of rapidly increasing q inside 1.25° radius (19.2 to 20.5 g kg^{-1}).

d. Radial variations in surface heat fluxes

Figure 7a illustrates surface fluxes of heat and moisture as a function of radial distance from the hurricane center. In addition to these values, Fig. 7a also illustrates sensible and latent heat flux estimates that assume SAC $= 1°$C and RH $= 85\%$. A statistical summary of these calculations is given in Table 4. The standard bulk aerodynamic expressions used to determine the fluxes of heat (H_S) and moisture (H_L) are

$$H_s = \rho C_p C_{H10}(\mathrm{SST} - \mathrm{TA}_{10})U_{10} \quad \text{and} \qquad (3)$$

$$H_L = \rho L_v C_{E10}(q_{\mathrm{SST}} - \mathrm{qA}_{10})U_{10}, \qquad (4)$$

where ρ is the density of air, C_p is the specific heat of air at constant pressure, L_v is the latent heat of vaporization at a given TA, TA_{10} is the air temperature at 10 m, U_{10} is the 1-min wind speed at 10 m, C_H and C_E are the dimensionless coefficients of heat exchange and moisture exchange at 10 m, while q_{SST} and qA_{10} and the saturation mixing ratio at the SST and the actual mixing ratio of the air at 10 m, respectively. Both C_H and C_E are assumed to be equal and are simply given by

$$C_{H10} = C_{E10} = (a + bU_{10}) \times 10^{-3}, \qquad (5)$$

where a and b are empirically determined constants with the values $a = 0.75$ and $b = 0.067$. These constants were chosen since they were determined under relatively high wind conditions >20 m s^{-1} (Garratt 1977; Black et al. 1988).

The latent and sensible heat flux profiles illustrated in Fig. 7a compare reasonably well with estimates made in previous studies (Riehl and Malkus 1961; Miller 1964; Machta 1969; Barnes and Powell 1995; Black and Holland 1995). Both the assumed and observed flux profiles in Fig. 7a depict rapid increases in total surface heat flux (sensible plus latent) near the inner core. Of particular significance is the observed increase in the TCBD-derived sensible heat flux inside 1.5° radius. (This trend is not observed for the assumed profile since SAC $= $ constant $= 1°$C.) This rapid rise in the relative contribution of surface sensible heat flux dramatically impacts the Bowen ratio near the inner core. An often-made assumption is that the Bowen ratio (defined as the ratio of sensible to latent heat flux) remains relatively constant with a value near 0.1 within the TC inflow layer (Huschke 1959; Hawkins and Imbembo 1976; Holland 1987). Figure 7b, however, shows that the observed Bowen ratio increases inside 2.5° radius and reaches a maximum average value of 0.20 near 0.5° radius. This significant increase in low-level diabatic warming in the inner core (when combined with nearly saturated conditions aloft) may help explain why surface air temperatures inside 1.25° radius remain relatively
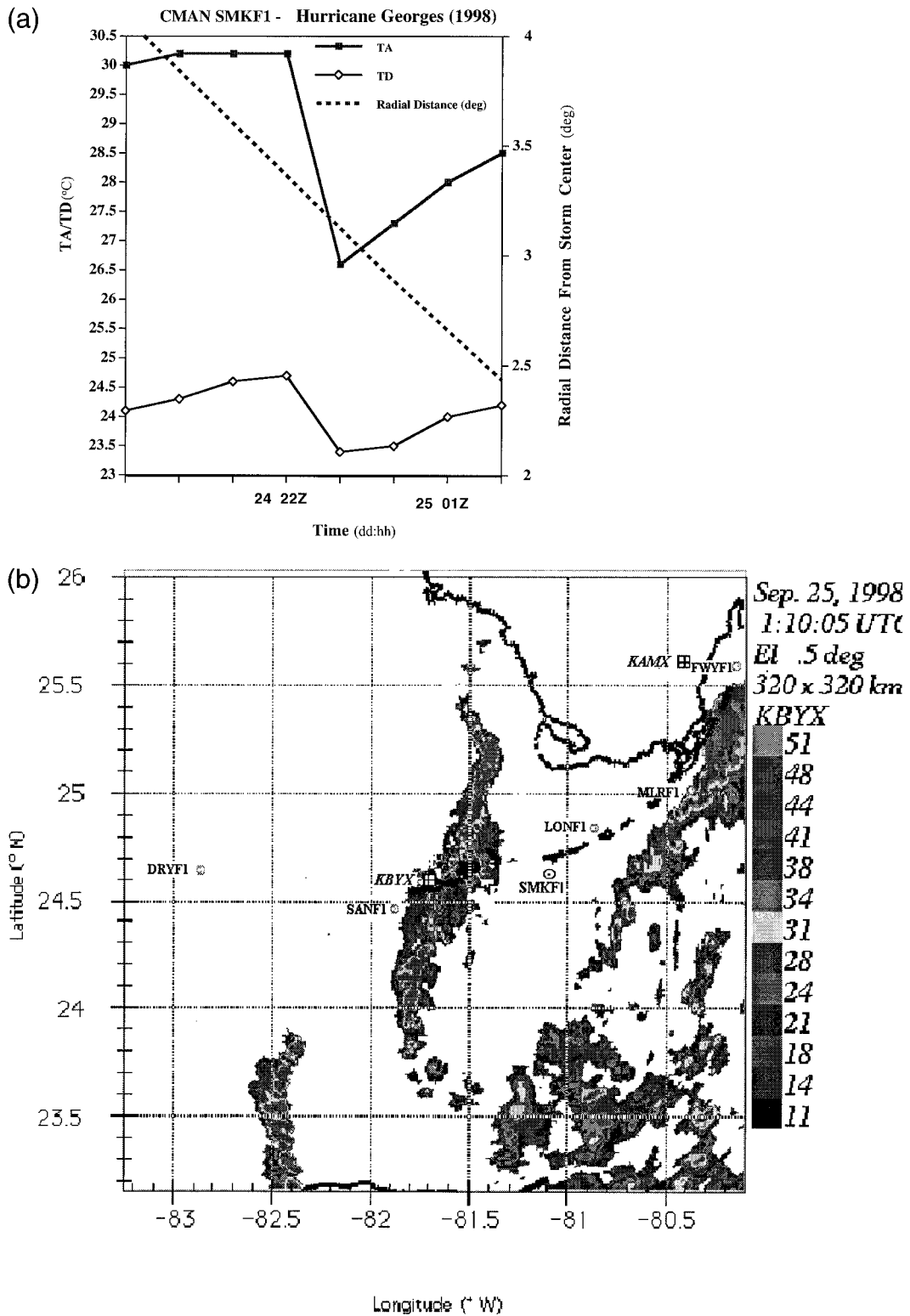
FIG. 5. (a) TA–TD partial time series from NDBC's SMKF1 C-MAN site during Hurricane Georges. The time series is valid between 1900 UTC 24 Sep and 0200 UTC 25 Sep 1998. The drops in TA (solid line–solid boxes) and TD (solid line–open diamonds) observed between 2200–2300 UTC on 24 Sep 1998 are associated with a strong line of convection that moved through the SMKF1 station. The distance of the SMFK1 station to the center of Hurricane
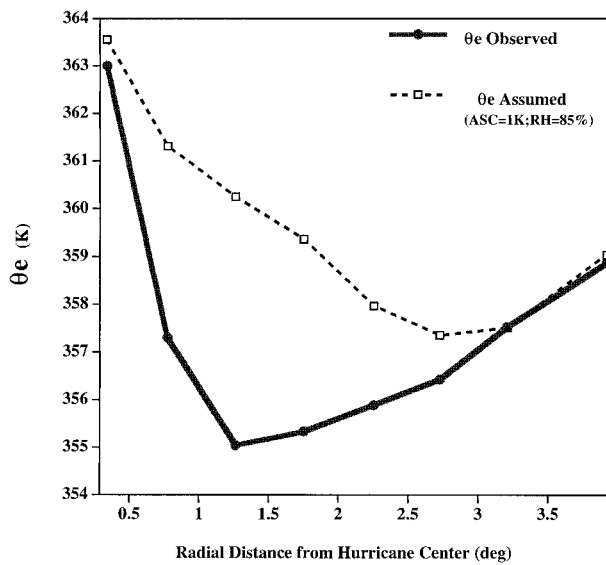
FIG. 6. The radially averaged composite θ_e profile for TCBD observations (solid line–solidcircles) and the θ_e profile calculated using the assumptions SAC = constant = 1°C and RH = constant = 85% (dashed line–open boxes).

constant despite strong surface winds, deep convection, and rapidly falling surface pressures.

4. Summary and conclusions

Composite analyses of surface data compiled from 37 Atlantic basin hurricanes between 1975 and 1998 suggest that the difference between observed sea and air temperatures increases significantly outside the hurricane inner core. Increases in sea–air contrast are much more common when the observed sea surface temperatures are at least 27°C. For this group of observations, most of the increase in sea–air contrast is a result of a reduction in air temperature and not an increase in sea temperature. These observations show that 90% of the total 2.1°C low-level cooling occurs 3.25°–1.25° radius from the hurricane center, far outside the region of strongest winds and horizontal pressure gradients. Adiabatic expansion of the inflowing air parcel only accounts for 16% of the cooling observed between 3.25° and 1.25° radius. It also appears that the observed reduction in air temperature is not simply a result of evaporation from sea spray or precipitation since the average surface specific humidity is observed to decrease 4.5°–1.75° radius from the composite storm center. A possible alternate explanation is that outside the inner core, unsaturated convective downdrafts are transporting relatively dry,
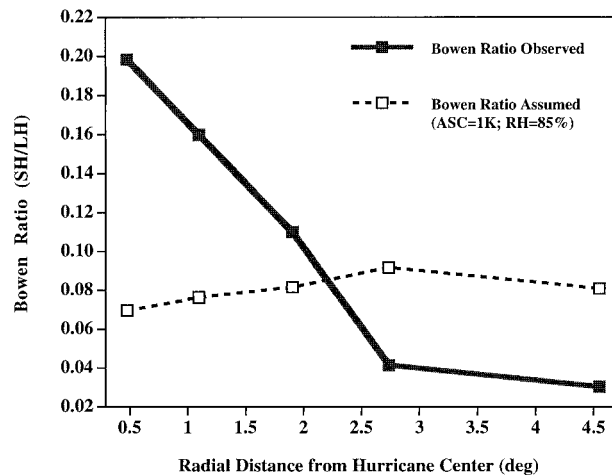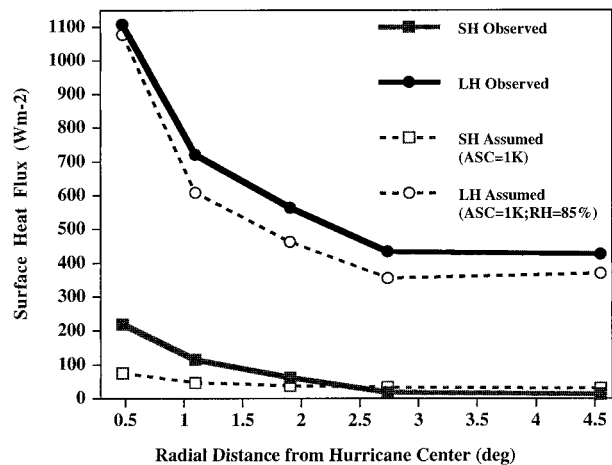

FIG. 7. (a) The radially averaged, surface sensible heat flux (SH) (solid line–solid boxes) and surface latent heat flux (LH) (solid line–solid circles) determined from TCBD observations. Also illustrated are SH flux (dashed lines–open boxes) and LH flux (dashed line–open circles) estimates that assume SAC = constant = 1°C and RH = constant = 85%. All surface fluxes illustrated are given in W m⁻². (b) The average Bowen ratio illustrated as a function of radial distance from the hurricane center. The Bowen ratio is defined as the ratio of SH flux to LH flux. The solid line represents average Bowen ratios obtained from TCBD observations while the dashed line is the Bowen ratio calculated using the assumptions SAC = constant = 1°C and RH = constant = 85%.

cool air into the near-surface environment. This low-level cooling and drying trend is also supported by earlier studies of tropical cyclone rainbands and squall lines. These studies illustrate that unsaturated downdrafts can act to significantly dry and cool the tropical

---

←

George is given in degrees radius and is illustrated as a dashed line. (b) Radar reflectivity from the National Weather Service's Key West site. This image is valid for 0110 UTC 25 Sep 1998 and depicts outer rainband structure associated with Hurricane Georges. Note that the westward moving line of convection centered in the illustration has passed through the SMFK1 station at this time. The reflectivity scale is illustrated to the right (in dBZ).

boundary layer within and near regions of active convection.

The near-surface composite analyses constructed in this research do not support conventional wisdom regarding the thermodynamic structure of the TC inflow layer. It is clear that inside 3.25° radius, the observed low-level inflow is not isothermal, constant with respect to surface specific humidity, or in thermodynamic near-equilibrium with the sea. Due to the observed low-level cooling and drying, calculated values of θ_e significantly decrease between 4.0° and 1.25° radius. However inside 1.25° radius, θ_e quickly recovers as surface pressures fall, specific humidity increases, and air temperatures remain relatively constant. On average, calculated surface sensible and latent heat fluxes are greater than fluxes that assume near-isothermal inflow and constant surface relative humidity. The greatest increase in surface sensible heat flux occurs inside 1.5° radius where surface winds are strong and sea–air temperature contrasts are large. This dramatic increase in low-level sensible heating (as well as a limited supply of dry air aloft in the inner core) may help explain why surface air temperatures inside 1.25° radius do not cool further despite strong surface winds, regions of active convection, and rapidly falling surface pressures.

The composite analyses used in this research incorporate much surface data from 37 hurricanes over a 23-year period. Still, additional near-surface thermodynamic observations and radar analyses of precipitation patterns are necessary in order to further refine the representation of the low-level thermodynamic environment presented in this research. It is hoped that additional observations obtained from future targeted dropwindsonde deployments (Hock and Franklin 1998) as well as flight-level measurements from aerosonde radial inflow experiments (G. Holland, 1999, personal communication) will play a pivotal role in dramatically improving the representation, physical understanding, and realistic simulation of the low-level hurricane environment.

REFERENCES

Barnes, G. M., and G. J. Stossmeister, 1986: The structure and decay of a rainband in Hurricane Irene (1981). *Mon. Wea. Rev.,* **114,** 2590–2601.

——, and M. D. Powell, 1995: Evolution of the inflow boundary layer of Hurricane Gilbert (1988). *Mon. Wea. Rev.,* **123,** 2348–2368.

——, E. J. Zipser, D. Jorgensen, and F. Marks Jr., 1983: Mesoscale and convective structure of a hurricane rainband. *J. Atmos. Sci.,* **40,** 2125–2137.

Betts, A. K., 1976: The thermodynamic transformation of the tropical subcloud layer by precipitation and downdrafts. *J. Atmos. Sci.,* **33,** 1008–1020.

Black, P. G., R. L. Elsberry, L. K. Shay, R. P. Partridge, and J. F. Hawkins, 1988: Atmospheric and oceanic mixed layer observations in Hurricane Josephine obtained from air-deployed drifting buoys and research aircraft. *J. Atmos. Oceanic Technol.,* **5,** 683–698.

——, and G. J. Holland, 1995: The boundary layer of Tropical Cyclone Kerry (1979). *Mon. Wea. Rev.,* **123,** 2007–2028.

Bolton, D., 1980: The computation of equivalent potential temperature. *Mon. Wea. Rev.,* **108,** 1046–1043.

Brown, J. M., 1979: Mesoscale unsaturated downdrafts driven by rainfall evaporation: A numerical study. *J. Atmos. Sci.,* **36,** 313–338.

Byers, H. R., 1944: *General Meteorology.* McGraw-Hill, 645 pp.

Emanuel, K. A., 1986: An air–sea interaction theory for tropical cyclones. Part I: Steady state maintenance. *J. Atmos. Sci.,* **45,** 1143–1155.

Fairall, C. W., J. D. Kepert, and G. J. Holland, 1994: The effect of sea spray on surface energy transports over the ocean. *Atmos. Ocean Syst.,* **2,** 121–142.

Fitzgarrald, D. R., and M. Garstang, 1981a: Vertical structure of the tropical boundary layer. *Mon. Wea. Rev.,* **109,** 1512–1526.

——, and ——, 1981b: Boundary-layer growth over the tropical ocean. *Mon. Wea. Rev.,* **109,** 1762–1772.

Frank, W. M., 1977: The structure and energetics of the tropical cyclone. I: Storm structure. *Mon. Wea. Rev.,* **105,** 119–1135.

——, 1984: A composite analysis of the core of a mature hurricane. *Mon. Wea. Rev.,* **112,** 2401–2420.

Garratt, J. R., 1977: Review of drag coefficients over oceans and continents. *Mon. Wea. Rev.,* **105,** 915–929.

Gilhousen, D. B., 1988: Quality control of meteorological data from automated marine stations. Preprints, *Fourth Int. Conf. on Interactive Information and Processing Systems for Meteorology, Oceanography, and Hydrology,* Miami, FL, Amer. Meteor. Soc., 113–117.

——, 1998: Improved real-time quality control of NDBC measurements. Preprints, *10th Symp. on Meteorological Observations and Instrumentation*, Phoenix, AZ, Amer. Meteor. Soc., 363–366.

Gray, W. M., and D. J. Shea, 1973: The hurricane's inner core region. Part II. Thermal stability and dynamic characteristics. *J. Atmos. Sci.,* **30,** 1565–1576.

Hawkins, H. F., and S. M. Imbembo, 1976: The structure of a small intense hurricane—Inez, 1966. *Mon. Wea. Rev.,* **104,** 418–442.

Hock, T. F., and J. L. Franklin, 1999: The NCAR GPS dropwindsonde. *Bull. Amer. Meteor. Soc.,* **80,** 407–420.

Holland, G. J., 1987: Mature structure and structure change. *A Global View of Tropical Cyclones,* R. L. Elsberry, Ed., Office of Naval Research., 13–52.

——, 1997: The maximum potential intensity of tropical cyclones. *J. Atmos. Sci.,* **54,** 2519–2541.

Huschke, R. E., Ed., 1959: *Glossary of Meteorology.* Amer. Meteor. Soc., 638 pp.

Johnson, R. H., and M. E. Nicholls, 1983: A composite analysis of the boundary layer accompanying a tropical squall line. *Mon. Wea. Rev.,* **111,** 308–319.

Jordan, C. L., 1952: On the low-level structure in the typhoon eye. *J. Meteor.,* **9,** 285–290.

——, 1958: Mean soundings for the West Indies. *J. Meteor.,* **15,** 91–97.

Jorgensen, D. P., 1984: Mesoscale and convective-scale characteristics of mature hurricanes. Part II: Inner core structure of Hurricane Allen (1980). *J. Amos. Sci.,* **41,** 1287–1311.

Korolev, V. S., S. A. Petrichenko, and V. D. Pudov, 1990: Heat and moisture exchange between the ocean and atmosphere in Tropical Storms Tess and Skip (English translation). *Sov. Meteor. Hydrol.,* **3,** 92–94.

Leary, C. A., 1980: Temperature and humidity in mesoscale downdrafts. *J. Atmos. Sci.,* **37,** 1005–1012.

Liu, W. T., K. B. Katsaros, and J. A. Businger, 1979: Bulk parameterizations of air–sea exchanges of heat and water vapor including the molecular constraints of the interface. *J. Atmos. Sci.,* **36,** 1722–1735.

Machta, J., 1969: Evaporation rates based on tritium measurements from Hurricane Betsy. *Tellus,* **21,** 404–408.

Malkus, J. S., and H. Riehl, 1960: On the dynamics and energy transformations in steady-state hurricanes. *Tellus,* **12,** 1–20.

Miller, B. I., 1958: On the maximum intensity of hurricanes. *J. Meteor.,* **15,** 184–195.

——, 1964: A study of the filling of Hurricane Donna (1960) over land. *Mon. Wea. Rev.,* **92,** 389–406.

Neumann, C. J., B. R. Jarvinen, C. J. McAdie, and J. D. Elms, 1993: Tropical cyclones of the North Atlantic Ocean, 1871–1992. Historical Climatology Series 6-2, National Climatic Data Center, Asheville, NC, 193 pp.

Palmen, E., 1948: On the formation and structure of tropical cyclones. *Geophysica,* **3,** 26–38.

Powell, M. D., 1990: Boundary layer structure and dynamics in outer rainbands. Part II: Downdraft modification and mixed layer recovery. *Mon. Wea. Rev.,* **118,** 919–938.

——, S. H. Houston, and T. Reinhold, 1996: Hurricane Andrew's landfall in south Florida. Part I: Standardizing measurements for documentation of surface wind fields. *Wea. Forecasting,* **11,** 304–328.

Pudov, V. D., 1992: The ocean response to the cyclones influence and its possible role in their track formations. *ICSU/WMO International Symposium on Tropical Cyclone Disasters,* WMO, 367–376.

——, and G. J. Holland, 1994: Typhoon and ocean: Results of experimental investigations. BMRC Research Rep. 45, Bureau of Meteorology Research Centre, Melbourne, Australia, 50 pp.

Riehl, H., 1950: A model of hurricane formation. *J. Appl. Phys.,* **21,** 917–925.

——, 1954: *Tropical Meteorology.* McGraw-Hill, 392 pp.

——, and J. S. Malkus, 1961: Some aspects of Hurricane Daisy (1958). *Tellus,* **13,** 181–213.

Simpson, R. H., 1978: On the computation of equivalent potential temperature. *Mon. Wea. Rev.,* **106,** 124–130.

Willoughby, H. E., 1995: Mature structure and evolution. *Global Perspectives on Tropical Cyclones,* R. L. Elsberry, Ed., WMO, 21–62.

Zipser, E. J., 1977: Mesoscale and convective-scale downdrafts as distinct components of squall-line activity. *Mon. Wea. Rev.,* **105,** 1568–1589.